

A Study of the Effects on Transmission Loss of Water Column Features as Modelled for an Area off the East Australian Coast

Adrian D. Jones (1), Alex Zinoviev (1) and Michael V. Greening (1)

(1) Defence Science and Technology Organisation, P.O.Box 1500, Edinburgh, South Australia 5111, Australia

ABSTRACT

The improved accuracy of ocean and atmospheric models permits the description of water column features, and sea surface wind stress, at a resolution which suggests employment in underwater acoustic transmission applications. In an investigation of aspects of linking modelled ocean data with range-dependent acoustic transmission models, a PE transmission code was used with data generated by the BLUElink suite of ocean and atmospheric models for a deep-water region off the east Australian coast for a particular summer period. The typical presence of warm and cold core eddies was found to result in a highly variable acoustic environment. Variations in expected range to particular levels of Transmission Loss were found to be mainly related to changes in the depth of the mixed surface layer, but also due to changes in the sound speed gradient in the thermocline. The study also made a brief consideration of the likely impact of wind speed variation over the region, and the effects of modelled ocean currents on acoustic transmission.

INTRODUCTION

It is well known that underwater sound is refracted, both in the vertical and in the horizontal, as a result of the presence of ocean features such as currents, eddies and fronts. It is expected that such mesoscale water column features may have substantial effects on sound transmission at frequencies less than, very approximately, 10 kHz, for which absorption effects do not dominate at distances of the order of the size of the features. This frequency range is relevant for many applications of underwater acoustic transmission. The recent developments in ocean modelling capability, such as BLUElink (Australian Bureau of Meteorology, n.d.), have provided 3-D gridded data, with vertical and horizontal resolutions of approximately several to tens of metres, and several to 10 km, respectively, with updates at intervals of hours, such that the necessary input description for an acoustic transmission model may be constructed. The present study was of the expected effects on undersea acoustic transmission due to the presence of ocean structures in the deep ocean region for which modelled data were available. Data used were from the SHOC model (Herzfield, 2012), which is part of the BLUElink modelling suite.

OCEAN REGION MODELLED

The study was limited to the examination of events modelled for a particular day in December 2011 for a region off eastern Australia including the coast from Eden to Newcastle, plus nearby deep regions. The region and time period were selected as they permitted the inclusion of a cold core eddy and two warm core eddies. The modelled Sea Surface Height Anomaly (SSHA) for the region is shown in Figure 1 for the time instant used for the study. This illustrates the location of the eddies and shows the surface current vectors modelled at 0.5 m depth, with the strongest vectors indicating a speed of about 1 m/s. An obvious feature is that the cold core eddy is associated with minimum height and cyclonic circulation, whereas the warm core eddies are associated with maximum height and anti-cyclonic circulation. Such characteristics of these eddy types are well known and anticipated.

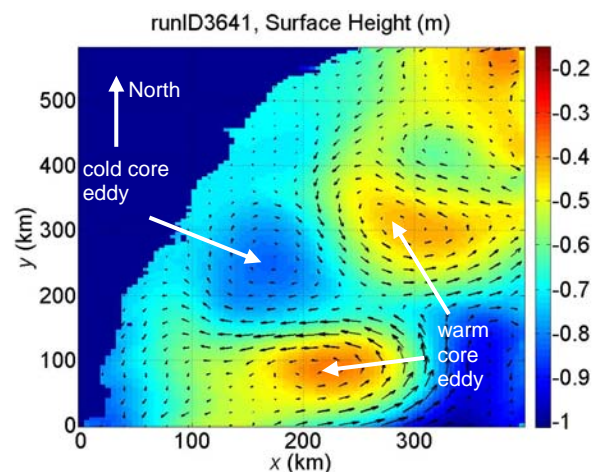


Figure 1. SSHA in region as modelled, showing location of eddies and surface currents

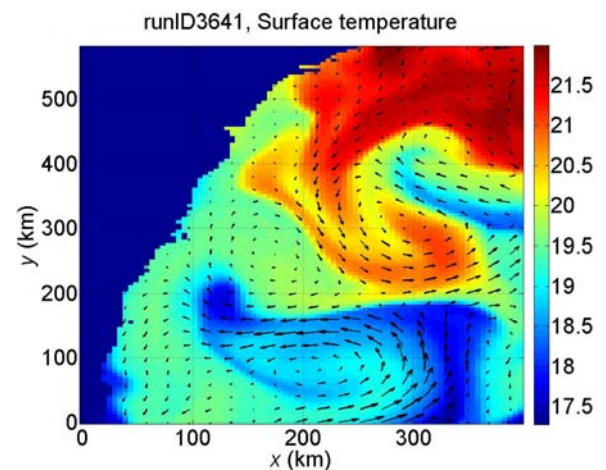


Figure 2. Sea surface temperature, °C, in region as modelled, showing location of eddies and surface currents

Figure 2 shows the contemporaneous sea surface temperature at 0.5 m depth, again including the surface current vectors at the same depth. For this example, which has been found to be typical, the location and type of each eddy correlates poorly with the features of the sea surface temperature. For example, in the figure, at the centre of the southern warm core eddy the surface temperature is lower than near the centre of the cold core eddy, which in turn is lower than at the centre of the northern warm core eddy.

ACOUSTIC MODELLING

Acoustic transmission modelling was carried out using the RAMGeo parabolic equation model (NRL n.d.). To highlight effects due to the water column features, the seafloor was modelled as absorptive, so that no bottom reflected acoustic energy was included. To further highlight water column features, acoustic reflection loss at the sea surface was not directly included in any modelling, nor was in-water absorption included. Calculations of Transmission Loss (*TL*) were carried out, centred at each grid point in latitude and longitude for which modelled water column data were available. Both range-independent calculations, using the single sound speed profile (SSP) existing at the nominal point of calculation and the depth value at that point, as well as full range-dependent calculations of *TL* using range-dependent bathymetry and SSP variations existing at points along the nominal track direction, were carried out. Determination of source to receiver ranges associated with particular values of *TL* was carried out over the entire region, for values of *TL* of 80 dB and 90 dB. The values of range shown in the following sections of this paper correspond with the longest range values associated with the phase-coherent *TL* of a nominal value, as obtained at any depth within the top 300 m of the ocean. This was used as a metric to highlight the effect of transmission variations that might be attributed to the ocean water column structure.

In this work, the source to receiver ranges were obtained for a source at (i) 20 m depth, and (ii) 70 m depth, at an acoustic frequency of 1.5 kHz. The ranges obtained using range-independent calculations are shown in Figures 3 and 4, for a *TL* of 80 dB, for the two source depths. The maximum range values shown are limited to 70 km, with greater values capped at that limit.

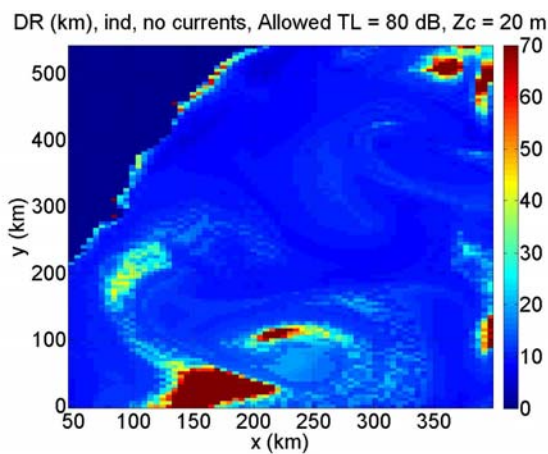


Figure 3. Maximum source to receiver range, in km, at any depth less than 300 m for range-independent *TL* of 80 dB, 1.5 kHz, source depth 20 m

The data in each of Figures 3 and 4 show a significant variation of range value at the different grid points over the ocean area, with the greater ranges, and very large variations in

range, being obtained for the sound source at 20 m depth. (Note that the contrast in Figure 4 is accentuated so that the range variations are clearly visible.) The reasons for these variations are explained in later sections, but it may be stated that the mesoscale features are the ultimate cause. As the range values for the source at 70 m depth are modest for a maximum *TL* of 80 dB, the data are re-drawn to a *TL* of 90 dB so as to accentuate effects discussed later.

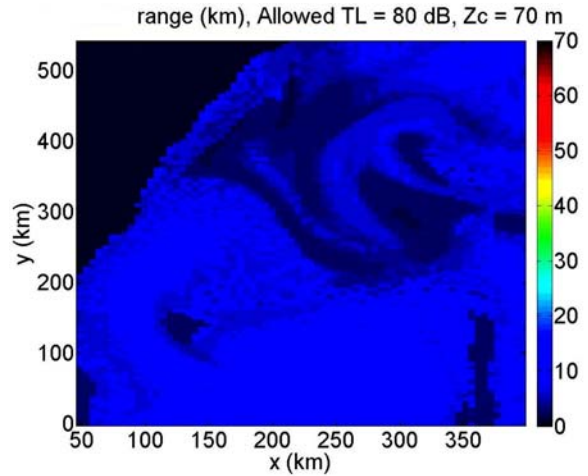


Figure 4. Maximum source to receiver range, in km, at any depth less than 300 m for range-independent *TL* of 80 dB, 1.5 kHz, source depth 70 m

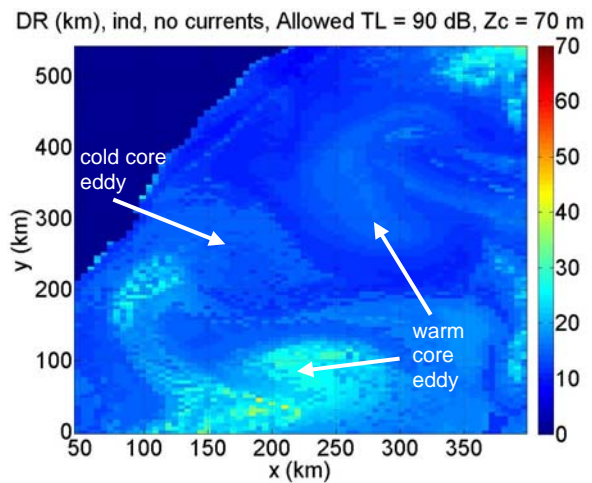


Figure 5. Maximum source to receiver range, in km, at any depth less than 300 m for range-independent *TL* of 90 dB, 1.5 kHz, source depth 70 m

MIXED SURFACE LAYER VARIATION

Surface Duct and Trapping Frequency Issues

As is well known, a region of well-mixed water may exist as a surface layer of the ocean, and is attributed to the recent history of weather events, including wind. Typically, the near-isothermal conditions in this layer exist on top of a decrease in temperature with depth in the region known as the thermocline, as shown in Figure 6. The upward refraction in the mixed layer is associated with the well-known phenomenon of an acoustic surface duct for which a trapping, or cut-off frequency, exists (e.g. Urick page 151 (1983)). At frequencies for which sound is “trapped” in the surface duct the propagation trends towards cylindrical spreading when the range is beyond a short transitional value (e.g. Urick page 152 (1983)).

The SSP in the thermocline results in downward refraction. If this SSP has a uniform gradient, as depicted in Figure 6, the sound paths will depict a series of circular arcs of uniform radius, so long as the angle of transmission is not large relative to the horizontal. Very approximately, the propagation within this region of circular arcs trends towards spherical spreading, for which the TL at a given range is higher than for cylindrical spreading. The resultant transmission for a particular scenario is then highly dependent upon whether the sound source is located in the surface duct or in the thermocline, and whether the surface duct supports trapping of the acoustic frequencies of interest.

Also of significance is whether the source is located within the surface duct and the receiver is below the duct. If this is the case, as illustrated in Figure 6, beyond a certain horizontal range, the receiver will be in a “shadow zone” and transmission loss will be very high.

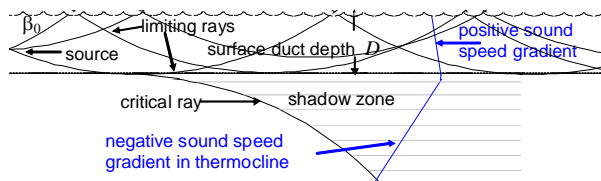


Figure 6. Sound transmission in mixed layer surface duct, over thermocline

The frequency for cut-off of the first acoustic mode within the surface duct, which is the lowest frequency f_{\min} to be trapped within the duct, may be determined as follows (e.g. Urlick page 151 (1983))

$$\lambda_{\max} = (8/3)\sqrt{2} \int_0^D \left(\sqrt{N(z) - N(D)} \right) dz \quad (1)$$

where $N(z)$ is the index of refraction at any depth z in the duct, $N(D)$ is the index of refraction at bottom of duct, D is surface duct depth, m , λ_{\max} is wavelength for first acoustic mode, m , $f_{\min} = c_w / \lambda_{\max}$ Hz, c_w is speed of sound in sea-water, m/s. It may be noted that Equation (1) is applicable to a sound speed gradient of any function of depth z , so long as the duct depth D is the depth corresponding to the maximum sound speed, below which the thermocline exists and sound speed reduces. For purposes of computation using Equation (1), if $N(z=D)$ is set to 1.0, $N(z) = c_{w,D} / c_{w,z}$, where $c_{w,D}$ is the speed of sound at depth D , and $c_{w,z}$ is the speed of sound at depth z . For all underwater applications, $N(z)$ is close to 1.0.

The basic phenomenon of duct trapping is well known, but some aspects are less known. Firstly, the well known Equation (1), which originates from the field of radar (page 20 of Freehafer and Kerr (Kerr 1951)) is not wave-based, but is determined from considerations of time-of-travel of limiting rays (see Figure 6) from one surface interaction to the next, a 180° phase shift on reflection at the surface, and a 90° phase shift at the turning point at the bottom of the duct at which a caustic is assumed to be formed. In the analysis of Freehafer and Kerr, the mode is formed by an in-phase re-enforcement that occurs as a limiting ray completes one surface skip. This cyclic re-enforcement is similar to that explained by Urlick (in his pages 174 – 175 (1983)) in relation to modes in isovelocity shallow water. As it originates from the concept of a limiting ray, Equation (1) implies perfect trapping of sounds at, and above, the frequency f_{\min} , however considering wave

effects this is not the case. For example, if a limiting ray is near to the centre of the streamline of acoustic energy, some of this will be within the thermocline and remain in it, thereby leaking from the duct.

No thorough explanation is given in this paper, but it may be stated that it is well known that leakage of acoustic energy into the thermocline is dependent on the SSP in the thermocline. Regardless, at the duct trapping frequency, f_{\min} , considerable leakage from the duct will occur, and the TL in the duct will be higher than indicated by the expectation of cylindrical spreading.

Simulations carried out using the SCOOTER wave-number integration model (Porter 2005), which incorporates all relevant physics, have shown that the leakage of energy from the duct is considerable at the duct trapping frequency, but is small if the frequency is sufficiently high to trap the second mode in the surface duct.

From Freehafer and Kerr (Kerr 1951), the trapping, or cut-off frequency for mode m is given by $f_{c,m} = c_w / \lambda_m$, where

$$\lambda_m = \left(\frac{2\sqrt{2}}{m-1/4} \right) \int_0^D \left(\sqrt{N(z) - N(D)} \right) dz. \quad (2)$$

For a surface duct with a uniform gradient $g \text{ s}^{-1}$ in the mixed layer, assuming that the variations in index of refraction $N(z)$ are very small, it is adequate to state that $N(z) = 1 + g(D-z)/c_{w,s}$. By performing the integration in Equation (2), it follows that the cyclic frequency $f_{c,m}$ of cut-on for mode no. m may be found from Equation (2) as

$$f_{c,m} = \frac{3(m-1/4)}{4\sqrt{2}g} \left(\frac{c_w}{D} \right)^{3/2} \quad m = 1, 2, 3 \dots \quad (3)$$

and so the cut-on frequencies for the first two modes are

$$f_{c,1} = f_{\min} = \frac{9}{16\sqrt{2}g} \left(\frac{c_w}{D} \right)^{3/2} \approx \frac{0.398}{\sqrt{g}} \left(\frac{c_w}{D} \right)^{3/2} \quad (4)$$

$$f_{c,2} = \frac{21}{16\sqrt{2}g} \left(\frac{c_w}{D} \right)^{3/2} \approx \frac{0.928}{\sqrt{g}} \left(\frac{c_w}{D} \right)^{3/2}. \quad (5)$$

Strictly, Equations (3) to (5) are in terms of sound speed at the surface $c_{w,s}$, however, for practical circumstances there is little variation in sound speed and any value c_w within the duct may be used, with little error.

Mixed Layer Surface Duct Features of SHOC data

Taking the depth of the mixed layer as corresponding with the maximum sound speed in the SHOC modelled data in the vicinity of the surface, depth values to a maximum of 60 m are shown in Figure 7. These determinations used the sound speed data which were included within the SHOC dataset, at each depth value at each grid point.

The data in Figure 7 indicate a considerable spatial variation, with a large total area existing over which the duct depth is less than 15 m. The SHOC data contains 4 depth values to

ocean depth 10 m, and 8 depth values to ocean depth 32 m, so it may be expected that the duct presence is suitably resolved. Of interest is the small region near the south part of the area for which a duct depth of 60 m or greater is nearby regions with much shallower depth.

A further indication of the variability in surface duct features over the modelled area is shown in Figure 8. This shows the average sound speed gradient, as determined from the change in sound speed throughout the duct divided by the duct depth. It is clear that this has a high spatial variability and is not necessarily the same as the value 0.017 s^{-1} expected for an isothermal duct.

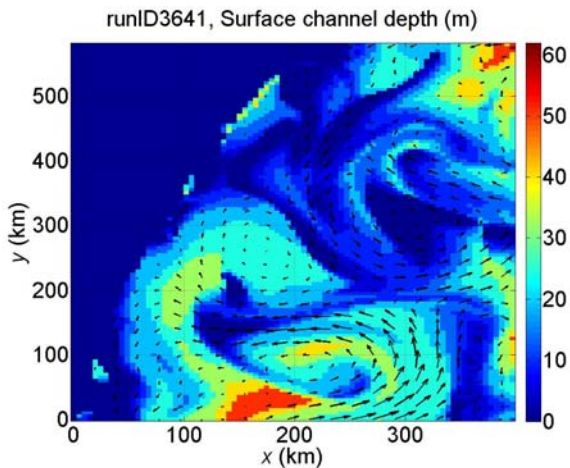


Figure 7. Depth of modelled mixed surface layer over region, surface currents shown

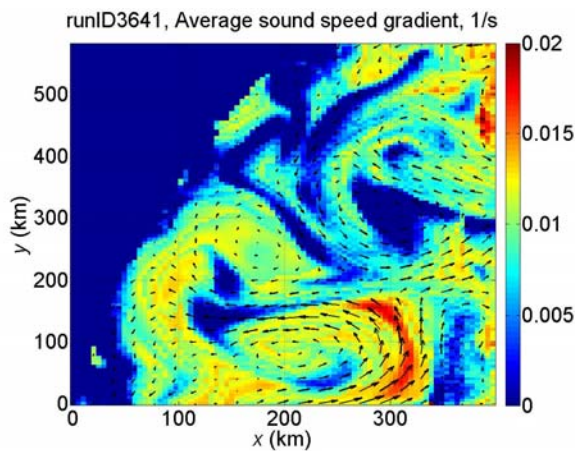


Figure 8. Average sound speed gradient in modelled mixed surface layer over region, surface currents shown

The corresponding cut-off frequencies, as determined from a numeric integration of the sound speed data in accord with Equation (1) are shown in Figure 9. The colour coding of Figure 9 has been arranged so that the dark red colour indicates a cut-off frequency of 3 kHz or greater. The figure then reveals only the areas for which the cut-off frequencies are below 3 kHz, and the dark red zones include areas for which the cut-off frequency may be much greater than 3 kHz. Surface current values at 0.5 m are shown so that the locations of eddies may be seen. A notable feature of the data is that most of the area has a cut-off frequency above 3 kHz, with a few smaller regions for which it is 1.5 kHz or less. By comparing the data in Figures 7 and 9 with the eddy locations in Figure 1, there appears to be no relation between the zones of good duct trapping and the presence of a particular type of eddy. As may be expected, however, the zones of reasonable

and good duct trapping at the frequency 1.5 kHz are highly correlated with the areas of best transmission for a source at 20 m depth, as shown in Figure 3.

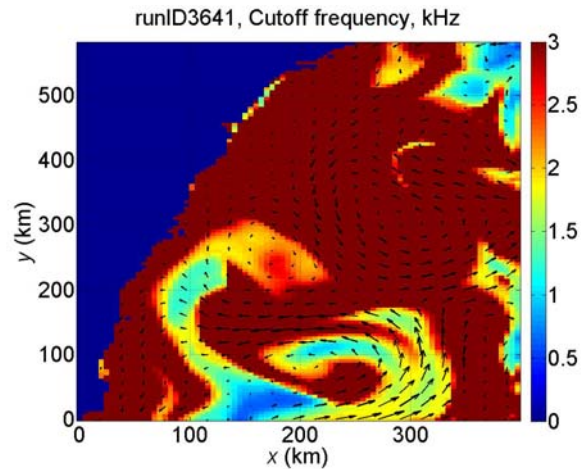


Figure 9. Variation of duct trapping frequency below 3 kHz for modelled mixed surface layer, surface currents shown

A careful examination of Figure 3 with reference to Figure 9 shows that the areas of best transmission (the dark red zones in Figure 3) correspond with a cut-off frequency of about 800 Hz or less. Assuming Equation (4) may be used to invert for a duct depth appropriate to a particular cut-off frequency, for 800 Hz, and for an average sound speed gradient of 0.014 s^{-1} (estimated from Figure 8), the duct depth is 39.1 m. From Equation (5) the frequency at which two modes will be trapped within a 39.1 m duct of sound speed gradient 0.014 s^{-1} is about 1.87 kHz. Thus in relation to the zones in Figure 3 corresponding with good transmission at 1500 Hz, the first mode may be considered well trapped (as corresponding cut-off frequency is 800 Hz) and the second mode will be contributing but leaking.

Areas coloured yellow in Figure 9, for which the cut-off frequency is about 1.8 kHz, correspond with zones of much poorer transmission at 1.5 kHz in Figure 3, even though this frequency is just slightly less than the cut-off. Lastly, areas in Figure 9 for which the cut-off is close to 1.5 kHz, coloured green, correspond with transmission in Figure 3 which is not as good as in the regions for which the duct trapping frequency is lower. Consideration of these data in Figures 9 and 3 does tend to confirm that the first mode in the duct must be well trapped, or two modes are required, for good transmission in the surface duct.

THERMOCLINE VARIATION

The variation of the sound speed gradient averaged from the bottom of the surface duct to the depth 250 m, is shown in Figure 10, together with the location of the warm and cold core eddies. It is well-known that the downward refracting sound speed gradient in the thermocline is maximised in the presence of a cold core eddy, and minimised in the presence of a warm core eddy. This is evident in the data, with a minimum gradient of the order 0.02 s^{-1} associated with the southern warm core eddy, and a maximum gradient of the order 0.085 s^{-1} associated with the cold core eddy.

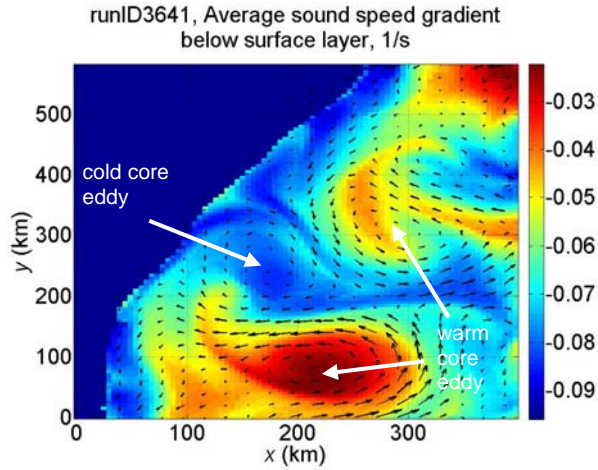


Figure 10. Gradient in modelled thermocline to 250 m depth, showing surface currents

Assuming that the sound speed gradient within the thermocline g_t is uniform, the transmission paths are downwardly refracted in the shape of circular rays of radius $c_w/(g_t \cos \beta)$, where β is the transmission angle relative to the horizontal. If angles β are relatively small, the relevant transmission is along arcs of circles of the same radius c_w/g_t . For a source at depth d_s the sound will travel to a receiver at depth d_r as shown in Figure 11, where it is here assumed that the surface duct is quite thin. It is simple to determine ranges r_1 and r_2 in terms of these depths and the sound speed gradient of the thermocline g_t , as follows

$$r_1 \approx \sqrt{2c_w d_r / g_t}, \quad r_2 \approx \sqrt{2c_w d_s / g_t}. \quad (6)$$

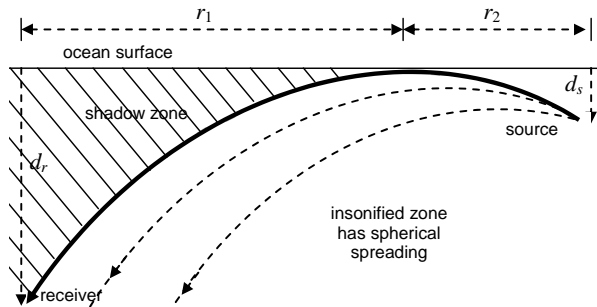


Figure 11. Ray transmission in thermocline, showing shadow zone, ocean with no surface duct

It follows from examination of Figure 11 that a shadow zone exists for receivers at ranges from the source greater than r_2 if they are located in the region above the ray that grazes the surface. For a receiver at depth d_r , if ray acoustics is presumed to apply, range $r_{\max} = r_1 + r_2$ is the maximum at which sound will travel to the receiver, as at greater ranges a receiver will be in a shadow zone, that is, the range to the shadow zone is

$$r_{\max} \approx \sqrt{2c_w/g_t} (\sqrt{d_r} + \sqrt{d_s}). \quad (7)$$

This ray acoustics-based analysis is an approximate estimate only, and sound will reach zones presumed to be in shadow, for example, through diffraction.

Based on Equation (7), for a source at various depth values, and receiver at any depth to 300 m, the maximum possible transmission ranges (which occur for receiver at 300 m depth) are shown in Table 1. These range values are determined for the extreme values of sound speed gradients determined from Figure 10, associated with the cold core eddy and the warm core eddy to the south of the region. The largest range value is for the source at the deepest depth, and for the smallest sound speed gradient, being 9.9 km.

Table 1. Transmission range as limited by thermocline shadow zone, receiver at 300 m

Source depth d_s	Thermocline gradient $g_t = 0.02 \text{ s}^{-1}$	Thermocline gradient $g_t = 0.085 \text{ s}^{-1}$
20 m	8.4 km	4.1 km
70 m	9.9 km	4.8 km

Within the ranges indicated by Table 1, for which direct sound transmission occurs, the spreading function may be assumed to be spherical. This follows as the transmission from the source may be approximated as existing along a series of circular arcs centred at the source. As the arcs all have the same radius, for small angles relative to the horizontal, the spreading at a range r will be similar to that from a series of straight line paths, that is it will be spherical with TL approximately $20 \log_{10} r$.

For the source at 70 m depth, the maximum TL in the insonified zone will then be expected to be 79.9 dB at 9.9 km range in the region of the warm core eddy, with much higher values beyond the insonified zone. Data in Figure 4 shows transmission ranges not much better than about 10 km for TL of 80 dB, which is somewhat in accord with the above simple analysis. However, Figure 5 shows ranges over 25 km being achieved at TL of 90 dB. This may be related to sound entering the shadow zones, e.g. through diffraction, but it is also likely that sound propagating via a leaking surface duct is contributing to the ranges indicated in Figure 5. Regardless, one of the zones in Figure 5 corresponding to the best transmission is that associated with the southern warm core eddy, as expected by the simple analysis.

RANGE-DEPENDENT EFFECTS

Range-dependent water column and bathymetry data

Full range-dependent modelling was carried out as described earlier, with examples being shown in Figures 12 and 13. Here the range-dependent transmission is modelled in the direction north from each grid point. Figure 13 shows the result when the horizontal speed of the current in the direction from south to north was added to the sound speed at each depth value at each grid point over the area. The corresponding calculation without current effects modelled, in Figure 12, is slightly different but not greatly so. Both these figures have, however, considerable differences with Figure 3, obtained with range-independent transmission loss.

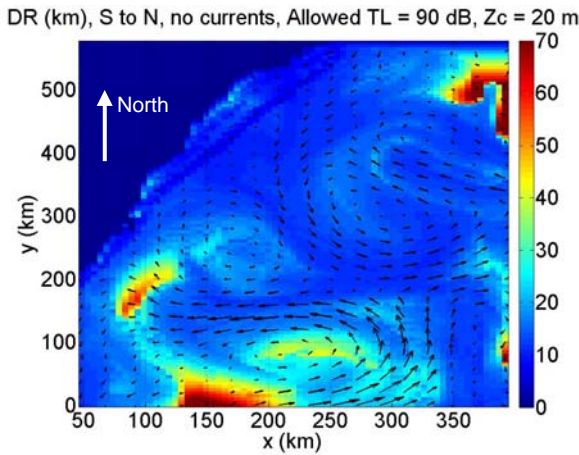


Figure 12. Maximum source to receiver range, in km, at any depth less than 300 m for range-dependent TL of 90 dB from south to north, 1.5 kHz, source depth 20 m

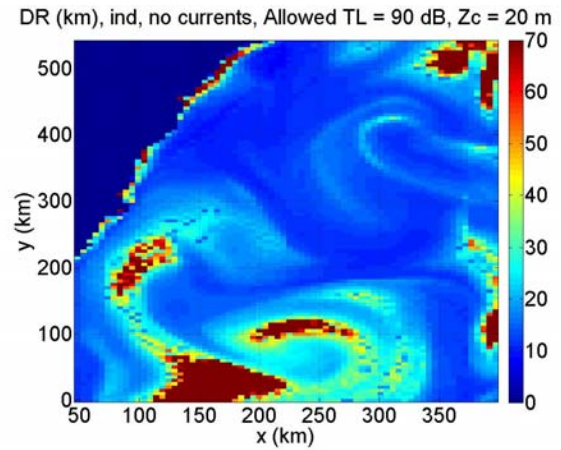


Figure 14. Maximum source to receiver range, in km, at any depth less than 300 m for range-independent TL of 90 dB, 1.5 kHz, source depth 20 m

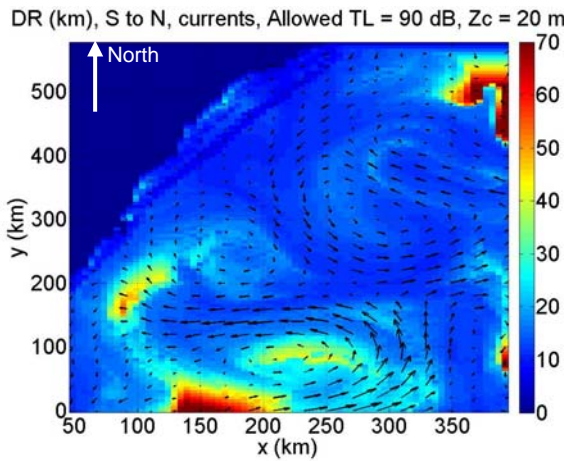


Figure 13. Maximum source to receiver range, in km, at any depth less than 300 m for range-dependent TL of 90 dB from south to north, 1.5 kHz, source depth 20 m, including effect of currents on sound speed

In order to make the most direct comparison with the range-independent transmission data in Figure 3, a similar figure showing the ranges for the same scenario, but for a value of TL of 90 dB, is shown in Figure 14. A general feature of this figure, in comparison with Figures 12 and 13, is that the apparent existence of zones of good transmission is exaggerated beyond the real, range-dependent, case. This occurs as the range-independent modelling is based on the local water column, and a water column conducive to good or very good transmission, due to either the surface duct or below layer gradient, is almost by definition likely to be bounded by zones with less favourable water columns. In detail, if the transmission range implied by range-independent modelling is of the order of, or larger than, ranges over which the water column varies significantly, there will obviously be differences between the results produced by the two types of modelling.

Range-dependent wind speed

Lastly, the wind speeds produced from the modelled sea surface wind stress data are shown in Figure 15.

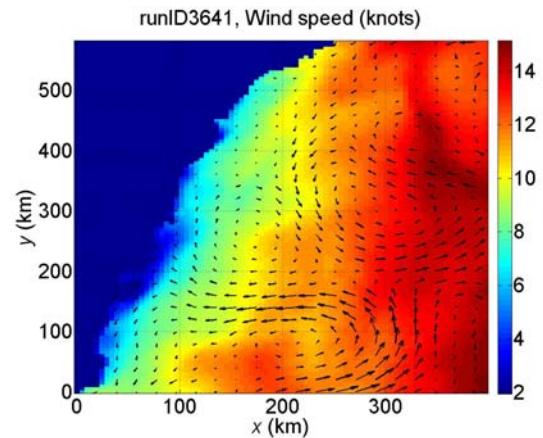


Figure 15. Modelled wind speed at 10 m above sea surface, knots, surface current shown

Here, magnitude of wind speed w_{10} m/s at the ocean surface, nominally at a height 10 m above it, is obtained from the ocean surface wind stress, τ Pascals, obtained from the SHOC data as

$$w_{10} = \sqrt{\tau / (\rho_a C_D)} \quad (8)$$

where ρ_a is the air density at the ocean surface and C_D is a drag coefficient, which for this work was obtained as (Trenberth 1989)

$$\begin{aligned} C_D &= (0.62 + 1.56/w_{10}) \times 10^{-3} \quad \text{for } w_{10} \leq 3 \text{ m/s} \\ &= 1.14 \times 10^{-3} \quad \text{for } 3 < w_{10} \leq 10 \text{ m/s} \\ &= (0.49 + 0.065 w_{10}) \times 10^{-3} \quad \text{for } w_{10} > 10 \text{ m/s} \end{aligned} \quad (9)$$

From Figure 15, the largest wind speed values are 15 kt (about 7.7 m/s). Values of coherent surface reflection loss were estimated using the JBZ model, described by Jones et al. (2012). This model incorporates the second-order small

slope model of roughness loss described by the Applied Physics Laboratory at the University of Washington (APL-UW), with a model of refraction in the bubbly region close to the surface taken from an exact solution to the wave equation. The latter effect results in a higher loss value than would exist in its absence, as it increases the angle of incidence at the surface. Surface reflection loss modelling has not been incorporated with the RAMGeo transmission modelling described earlier, but separate application of the JBZ model has shown that for a wind speed of 7.5 m/s, the loss at 1.5 kHz for sound received in a surface duct of 64 m thickness from a source at 18 m depth is close to 0.05 dB/km, averaged over a long range. For transmission to a range of 70 km, the maximum value shown in Figures 3, 12, 13 and 14, the additional loss due to surface reflections in a surface ducted environment, will then be no greater than about 3.5 dB. This compares with about 0.085 dB/km due to in-water absorption in seawater at 20°C (Urick's fig 5.5 (1983)). For transmission at higher frequencies (e.g. half an octave higher and more), there are increases in each of in-water absorption and surface reflection loss in a surface ducted environment, on a dB/km basis, and it may be shown that the rise in the latter eventually outstrips the rise in the former, although both need to be included in either range-dependent or range independent modelling.

CONCLUSIONS

This study investigated the effects on modelled acoustic transmission due to the presence of ocean water column features described by the SHOC model within the BLUElink ocean modelling system for a sample dataset for the deep ocean off Australia's east coast in the summer period. For sound sources located at shallow depths, the most significant effect on sound transmission for the subject dataset, was the presence, or absence, of a mixed layer surface duct and the relationship between the trapping frequency and the acoustic frequency, when the sound source was in the duct. For a given level of Transmission Loss of the order of 80 dB, the associated transmission range was greatest if the duct trapping frequency was of the order of half the sound frequency of interest, or less. For regions in which the duct trapping frequency exceeded the sound frequency, very poor transmission resulted. A sound frequency about the same as the duct trapping frequency resulted in transmission of an intermediate quality. Although neither surface reflection losses nor in-water absorption effects were included in this modelling, at the frequency of interest these effects were judged to be very small.

For a sound source located below the surface duct, or in the absence of a surface duct, the most significant effect on sound transmission was the strength of the downward refracting sound speed gradient in the thermocline beneath the surface duct. For source and receiver both located below the surface duct, the weaker gradient associated with a warm core eddy resulted in a larger detectable range for which the limitation is likely to be the shadow zone as described by simple ray acoustics.

In general, there was a significant difference between transmission ranges implied by range-dependent versus range-independent modelling, with the latter having the potential to give a misleading view of greater range. Based on the limited work in this study there did not appear to be any benefit achieved by the inclusion of the water speed due to ocean currents in the determination of effective sound speed within the water column.

ACKNOWLEDGEMENT

The SHOC data used in this study were provided by staff within the Hydro METOC Branch of the Australian Hydrographic Office.

REFERENCES

- Australian Bureau of Meteorology, n.d., <<http://www.bom.gov.au/blueink/>>
- Herzfield, M. and Waring, J. R., 4 May 2012, *SHOC Sparse Hydrodynamic Ocean Code V4024 User Manual*, CSIRO Marine Research
- Jones, A.D., Duncan, A.J., Bartel, D.W., Zinoviev, A. and Maggi, A.L., 2 – 6 July 2012, 'A Physics-Based Model of Surface Reflection Loss for Ray Models', *Proceedings of the 11th European Conference on Underwater Acoustics*, Edinburgh UK, pp 77 – 84
- Kerr, D. E., ed., 1951, *Propagation of Short Radio Waves*, McGraw-Hill
- NRL n.d., <<ftp://ftp.ccs.nrl.navy.mil/pub/ram/RAM/>>
- Porter, M. B. 2005, Acoustic Toolbox, <<http://www.hlsresearch.com/oalib/Modes/AcousticsToolbox>>
- Trenberth, Kevin E.; Large, December 1989, William G. and Olson, Jerry G., *The Effective Drag Coefficient for Evaluating Wind Stress over the Oceans*, Journal of Climate, pp 1507 - 1516
- Urick, R.J. 1983, *Principles of Underwater Sound*, 3rd edition, Peninsula Publishing, Los Altos